Earth and Space Science

TECHNICAL REPORTS: METHODS
10.1029/2019EA000783

Calibration of Differential Pressure Gauges Through in Situ Testing

A.K. Doran[1], M. Rapa[1], G. Laske[1], J. Babcock[1], and S. McPeak[1]

[1]Scripps Institution of Oceanography, University of California San Diego, La Jolla, California

Key Points:
- We calibrated differential pressure gauges (DPGs) at seafloor pressures and temperatures
- DPGs exhibit departures from the nominal instrument response with regards to both sensitivity and time constant
- Devices like those described here could provide a cost-effective way to individually calibrate DPGs and improve the utility of DPG data

Supporting Information:
- Supporting Information S1

Correspondence to:
A. K. Doran,
adoran@ucsd.edu

Citation:
Doran, A. K., Rapa, M., Laske, G., Babcock, J., & McPeak, S. (2019). Calibration of differential pressure gauges through in situ testing. *Earth and Space Science*, *6*. https://doi.org/10.1029/2019EA000783

Received 3 JUL 2019
Accepted 28 OCT 2019
Accepted article online 3 DEC 2019

Abstract Differential pressure gauges (DPGs) are a standard component of modern broadband ocean-bottom seismometer instruments and have proven useful for observing a wide range of seismic and oceanographic phenomena. However, the response function of the DPG remains poorly known, limiting our ability to recover amplitude and phase information from seafloor pressure signals with high fidelity. The sensitivity and long-period response are difficult to calibrate in the lab, as they are known to vary with temperature and pressure and perhaps between sensors of the same design. We present the results of a field experiment designed to determine empirical response functions *in situ* by inducing a pre-defined pressure offset on a deployed instrument. The results compare favorably with calibrations estimated independently through post-deployment data analyses. Our study demonstrates that observed response functions can deviate from the nominal response by a factor of two or greater with regards to both the sensitivity and the time constant. Incorporating calibration devices such as those described here into future deployments may prove to be a cost-effective way to improve the accuracy and utility of differential pressure data.

1. Introduction

The Cox-Webb differential pressure gauge (DPG; Cox et al., 1984) was developed to measure fluctuations in seafloor pressure with a dynamic range of three decades over a broad frequency band (spanning mHz to Hz) by measuring the difference between ocean pressure and the pressure within a reference chamber of viscous oil. Although insensitive to absolute pressures, DPGs have significantly lower noise floors than most other pressure gauges (approaching or below 0.01 Pa^2/Hz) and are now regularly included in modern broadband ocean-bottom seismometer (OBS) deployments. Seafloor pressure data have been used for applications as diverse as seismic imaging (e.g., Crawford et al., 1991; Crawford & Webb, 2002; Doran & Laske, 2016, 2019; Laske et al., 1999, 2007; Weeraratne et al., 2007), earthquake seismology (e.g., An et al., 2017), tsunami modeling (e.g., Gusman et al., 2016; Melgar & Boch, 2013; Saunders & Haase, 2018; Sheehan et al., 2015), measurements of infragravity waves (e.g., Godin et al., 2013, 2014), improving signal-to-noise ratios on vertical seismic components (e.g., Bell et al., 2015; Crawford & Webb, 2000; Webb & Crawford, 2010), seafloor geodesy (e.g., Bürgmann & Chadwell, 2014; Nooner & Chadwick, 2016; Sasagawa et al., 2016) and studies of marine mammals (e.g., Wilcock et al., 2014).

Despite these successes, uncertainties in the response function, which describes the conversion of raw counts to physical units of pressure, continue to limit the utility of DPG data. Recording the amplitude of seafloor pressure signals is crucially dependent on accurate response information. The response of the modern Scripps Institution of Oceanography (SIO) DPG is characterized by two parameters: a sensitivity (or gain) constant k_0, describing the overall sensitivity of the system to changes in seafloor pressure, and a time constant τ, which describes the relaxation time of the system as the reference chamber slowly equilibrates with ambient ocean pressure and thereby controls the long-period response of the instrument (see Supporting Information and Figure S1 for details). The response function is typically represented in a complex poles and zeros format, with one zero defined at $z = (0 + 0i)$ and the real part of one pole defined by the inverse of the time constant, such that $p = (1/\tau + 0i)$. To date, the sensitivity and the time constant are both poorly calibrated at seafloor temperatures and pressures and are difficult to measure in the lab. The current nominal time constant of 79.57 sec/rad, measured by Willoughby et al. (1993), is subject to ongoing debate and is suspected to vary between individual instruments. Recently, techniques have been developed to determine the instrument sensitivity during data post-processing (e.g., An et al., 2017; Zha & Webb, 2016), but such calibrations are often

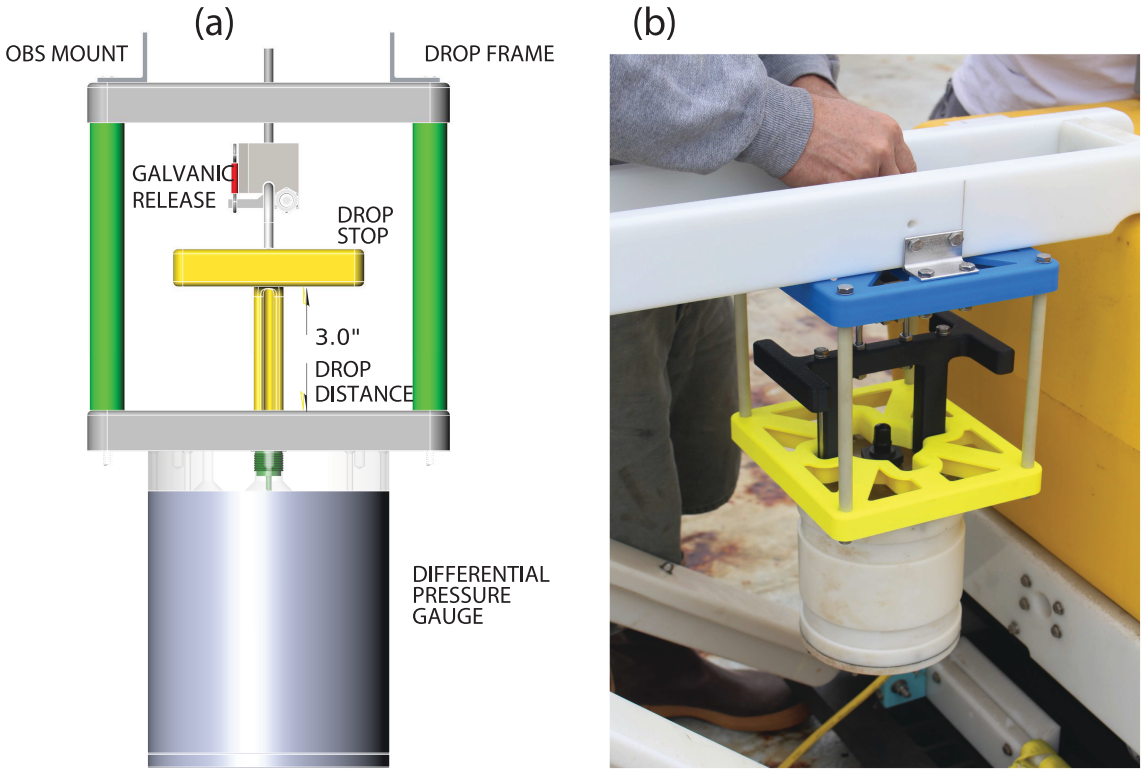

Figure 1. (a) Diagram of DPG drop mechanism. After 44-60 hours of continuous recording on the seafloor, the galvanic release dissolved and the DPG descended three inches (7.62 cm) until the drop stop collided with the bottom of the drop frame. The resulting signal was used to calibrate three DPGs *in situ*. (b) Photo of DPG drop mechanism attached to the OBS arm. The DPG is contained in the white cylinder, the drop frame is blue and yellow, and the drop stop is black

undertaken concurrently with the analysis of other seismic observables, may be biased by inaccurate models of oceanic or crustal properties, and are difficult to verify independently.

We present the results of an experiment conducted to measure the sensitivity and time constant of DPGs while the instruments were continuously recording on the seafloor. A DPG calibration device (Figure 1) was designed to control a precise depth change of 3 inches (7.62 cm). The device was designed by 3D modeling and produced by printing from ABS plastic. The main frame of the device was attached to the arm of the OBS frame using stainless steel bolts and brackets. The DPG was attached to the drop stop portion of the device using stainless bolts and suspended 3 inches above a base plate using a galvanic release. The OBS was deployed, and after the dissolution of the galvanic release was complete, a stainless-steel latch opened, releasing the drop stop and attached DPG. The sensor then dropped vertically until the drop stop feature contacted the base plate, completing the total depth change of 3 inches.

We conducted tests on three instruments deployed during the summer of 2018 off-shore in local waters. Two additional instruments without calibration devices were included in the deployment and allowed additional comparisons. We found that individual response functions can vary from the nominal response by a factor of two or greater with regards to both the sensitivity and the time constant. We compared our results to calibrations obtained during data post-processing. Specifically, we analyzed the pressure-acceleration transfer function during teleseismic Rayleigh wave arrivals as described by Zha and Webb (2016) to determine the instrument sensitivities and we compared observed and predicted tidal signals to constrain the time constants. Our results demonstrate the range of response functions exhibited by nominally identical DPGs and suggest that *in situ* tests may be necessary to accurately calibrate differential pressure data.

2. Observations

Five broadband OBS instrument packages were deployed during a test cruise in the San Clemente Basin of the California Borderland for over three months beginning in June 2018 (Figure 2). The instruments were

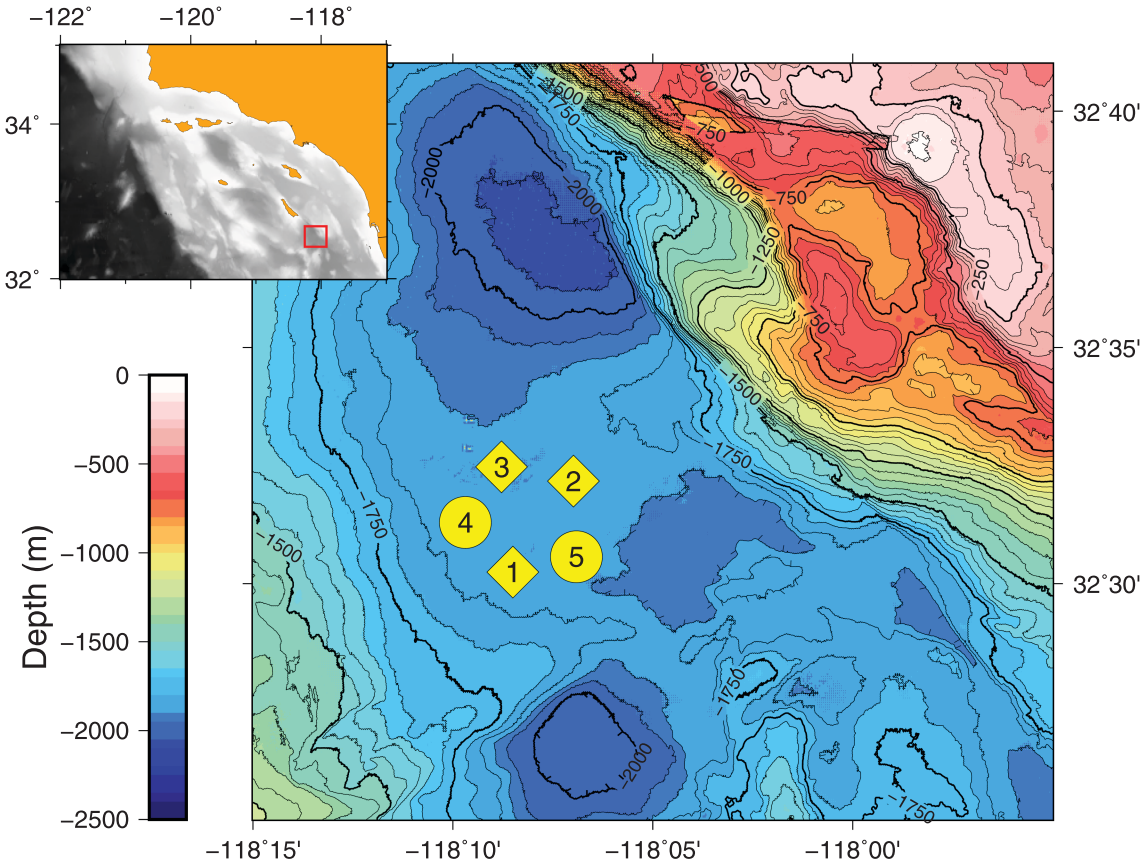

Figure 2. Location map of the five instruments deployed during this experiment. Instrument packages with DPG drop mechanisms (SCB1, SCB2, and SCB3) are represented with diamonds. Bathymetry data are from Smith and Sandwell (1997)

situated at ocean depths between 1600 and 2000 meters (as measured during deployment) and were arranged with an array aperture of ~5 km. Each package contained a three-component Nanometrics Trillium T240 seismometer, with a flat velocity response from 35 Hz to periods of 240 seconds, and a Cox-Webb DPG. These instruments are essentially the same instruments as provided for the NSF-funded OBS Instrument Pool (OBSIP; see www.obsip.org). All components recorded continuously at 100 samples per second (sps). Three of the five instruments (SCB1, SCB2, and SCB3) were equipped with DPG calibration mechanisms as described above. The drops initiated following 44-60 hours of recording data on the seafloor and occurred over the span of approximately 0.3 seconds. The instruments were wired such that an increase in pressure produced a negative pulse, which should be accounted for in the instrument response. Assuming an average seawater density of ρ =1028 kg/m^3, as found by Berelson (1991) in neighboring basins of the California Borderland, a three inch drop produced a pressure offset of 768.2 Pa.

We estimated the sensitivity of each DPG (Figure 3) by measuring the difference in counts produced by the drop, converting the count value to Pascals assuming the nominal sensitivity, and comparing this measurement with the expected pressure offset. The pre-drop count value was determined using the median of the 50 samples (0.5 seconds) preceding the drop. Because the DPG re-equilibration began instantly, we solved for the post-drop count value by examining data segments varying in length between 50 and 300 samples following the completion of the drop. A least-squares regression was used to solve for a linear fit to each segment and the count value at the intercept of the recovery was determined. We took the median of these values as the post-drop count estimate. Rather than simple averaging, we used this approach to avoid biasing the offset count while the sensor re-equilibrated. The uncertainty of the drop measurement was calculated as the square root of the sum of the individual count measurement uncertainties squared. For example, at SCB3 we measured an offset of 994597 ± 13174 counts. After multiplying this by the nominal sensitivity and

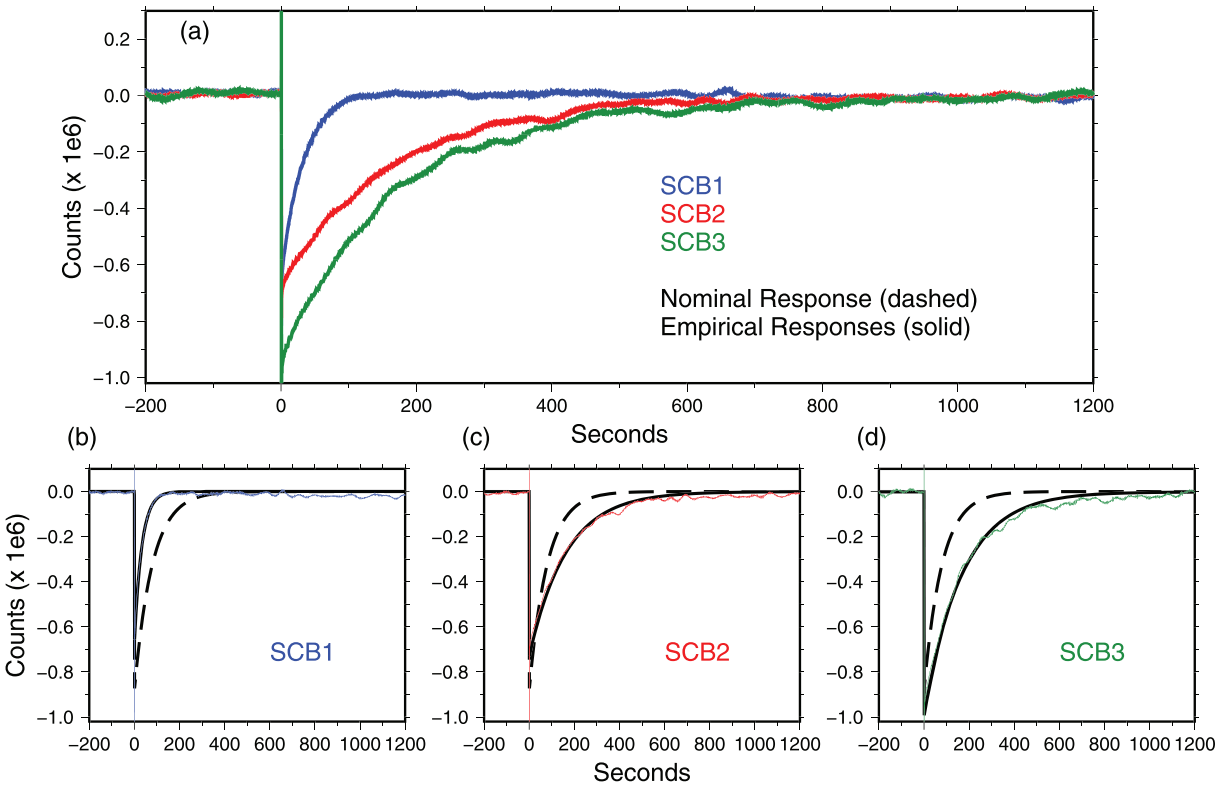

Figure 3. (a) Data recorded at stations SCB1, SCB2, and SCB3 before and after the DPG drop. While the drops occurred at different times for each instruments, the data have been aligned on the onset of each descent. (b) - (d) Drop data at each station compared to the expected signal produced by the nominal instrument response (dashed black line) and the best-fitting empirical response (solid black line)

dividing by the expected offset, we found a sensitivity correction factor of 1.13 ± 0.02. In our analyses, a correction factor greater than 1 indicates the instrument sensitivity was too high, and count values must be reduced by such a factor. At SCB1 and SCB2, we found factors of 0.75 ± 0.01 and 0.83 ± 0.01, respectively. Between the three drop instruments, the sensitivities varied by over 50%.

To determine the empirical time constant of the instruments, we modeled the drop as a step function linearly decreasing from 0 to -768.2 Pa over the duration of the descent. The data were demeaned by removing the median value calculated in the 50 samples preceding the drop. We applied the sensitivity-corrected instrument response to the step function and solved for the time constant that produced the lowest data misfit, defined as the L2 norm of the data minus the model in a ten minute window following the DPG drop. At SCB3, this yielded a best-fitting time constant of 168.2 sec/rad (Figure 3). Uncertainties were determined by repeating the fit while assuming the lower and upper sensitivity bounds (e.g., 1.11 and 1.15 at SCB3) and using twice the resulting range of time constants, leading to a range of $162.6 \leq \tau \leq 175.2$ sec/rad. Note that a larger sensitivity value yielded a smaller time constant, and vice versa. The results were insensitive to small changes to the modeled descent duration (i.e., between 0.3 and 1.0 seconds). Solving for the minimum misfit in a 15-minute window led to a preferred time constant of 170.3 sec/rad, consistent with our previous fit. Using the same procedure with 10 minute windows, we found best-fit time constants of 32.3 ($31.7 \leq \tau \leq 33.1$) sec/rad at SCB1 and 163.6 ($159.6 \leq \tau \leq 167.8$) sec/rad at SCB1 and SCB2 (Figure 3). All three results showed significant departure from the nominal value of 79.57 sec/rad. Final calibration values are shown in Figure 4.

3. Comparison with alternative calibration techniques

We compared our *in situ* calibration results to those obtained through alternative post-processing methods. The sensitivity of a DPG can be estimated by examining the transfer function between pressure and

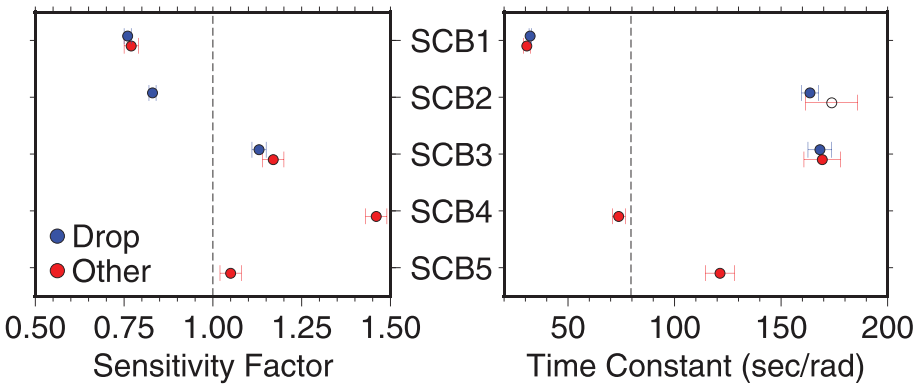

Figure 4. Final sensitivity and time constant estimates at each station using the drop data (blue symbols) and the data processing techniques (red symbols). Nominal values for sensitivity and time constant value are shown with the black dashed lines. The sensitivity at SCB2 could not be estimated using the method of Zha and Webb (2016) because the vertical seismometer component failed. We estimated the time constant assuming the sensitivity factor determined by the drop calibration

acceleration recorded during teleseismic earthquakes. Filloux (1983) first recognized that for slow motions at long periods, at which the compressibility of seawater is negligible, the pressure signal (P) generated by a seismic disturbance results from the vertical acceleration of the water column, and therefore $P = \rho ha$, where ρ is the density of seawater, h is the water depth, and a is the seafloor acceleration. Ball et al. (2014) used this formulation to calibrate sensors by calculating the transfer functions during Rayleigh wave trains at periods around 30 seconds. Zha and Webb (2016) extended this theory to higher frequencies, at which the theoretical transfer function is weakly dependent on the velocity of sound in water (α) and the local phase velocities of the Rayleigh wave c as a function of angular frequency (ω):

$$\frac{P}{a}(\omega) = \frac{\rho \sin(rH)}{r\cos(rH)}, r(\omega) = w\left(a^{-2} - c(\omega)^{-2}\right)^{1/2}$$

Here we assumed α = 1500 m/s, ρ = 1028 kg/m^3, and phase velocities from Laske and Widmer-Schnidrig (2015), calculated from the PREM mantle model (Dziewonski & Anderson, 1981) overlain with oceanic crust. We examined seven events with Mw > 6 and a source depth less than 150 km that occurred during the deployment (Table S1). Spectra and transfer functions were computed using thirty-minute data windows (tapered with a Hanning function) centered on the predicted arrival time of the 40 mHz Rayleigh wave packet (method modified from Doran & Laske, 2017). Acceleration spectra varied by 1-2% between stations, while the pressure spectra varied by over 40%, suggesting that variations in the transfer functions were primarily caused by variations in DPG instrument responses (Figure S2). We computed final median transfer functions at each station using all events that produced high pressure-acceleration coherence (> 0.95) at 50 mHz. Seven events were included at SCB3, five at SCB1 and SCB5, and four at SCB4 (Table S1). We determined the least-squares solution for the best-fit constant offset between the observed and predicted transfer functions between 40 and 80 mHz (Figure S3). Uncertainties were determined as the median standard deviation of the transfer functions at each frequency. Different window lengths (ranging from 10 to 40 minutes) led to variations in the inferred sensitivity on the order of 1%. The sensitivity values at SCB1 (0.77 ±0.02) and SCB3 (1.17 ± 0.03) are consistent with those determined using the drop data. We were unable to estimate the transfer function and overall sensitivity at SCB2, as the vertical seismometer component of this instrument malfunctioned for the duration of the deployment. The sensitivity values at SCB4 (1.46 ±0.03) and SCB5 (1.05 ± 0.03) demonstrate an even greater range (exceeding a factor of two) of sensitivities exhibited by individual DPGs. This large range of sensitivities is consistent with the ranges reported by Zha and Webb (2016) and Doran and Laske (2019).

Empirical time constant values were estimated by comparing the observed long-period pressure spectra to predicted tidal spectra. Although outside the nominal operational range of DPGs, tidal signals are routinely observed on DPGs in the deep ocean (e.g., Laske, 2011; Sheehan et al., 2011, 2015). A time series of expected

tidal amplitudes within the array (118.1417 W, 32.5041 N) was computed at a sampling rate of 30 minutes using the OTPS software of Egbert and Erofeeva (2002). We used the OSU tidal model (TPX07) and included tidal constituents M2, S2, N2, K2, K1, O1, P1, Q1, Mm, and Mf. Tidal amplitudes were converted to Pa assuming a seawater density of 1028 kg/m^3. We calculated observed amplitude spectra at all sites using two weeks of data. Data were zero-phase filtered using a 8-pole low-pass Bessel filter with a corner period at 2 hours, down-sampled to a 30-minute sampling interval, and tapered with a Hanning function (Figure S4). Although both the semi-diurnal and diurnal tidal signals were visible in the observed spectra, we analyzed the semi-diurnal signal because it was recorded with twice the spectral amplitude. We determined the time constant value that minimized the least-squares residual between the observed and expected amplitude spectra (corrected for sensitivity) at a triplet of discrete frequencies surrounding the central peak at 0.0223 mHz, the frequency closest to that of the semi-diurnal M2 tide (e.g., Wahr, 1995). Uncertainties in the time constant were again estimated as twice the range produced by assuming the range of sensitivity correction values. At SCB1 and SCB3 we found time constants of 30.8 ($29.4 \leq \tau \leq 32.6$) sec/rad and 169.3 ($160.7 \leq \tau \leq 178.1$) sec/rad, consistent with the drop results but with larger uncertainties. At SCB2, using the sensitivity found by the drop and an uncertainty of ± 0.03, typical of the transfer function uncertainties, we found a pole value of 173.7 ($161.1 \leq \tau \leq 190.7$) sec/rad, also consistent with the drop response. At SCB4 and SCB5 we found intermediate values, with time constants of 73.9 ($70.9 \leq \tau \leq 76.9$) sec/rad and 121.3 ($114.5 \leq \tau \leq 128.3$) sec/rad, respectively. We obtained consistent results at all stations after repeating the analysis with data filtered with an 8-pole Butterworth filter and average amplitude spectra computed using orthogonal Slepian multi-tapers (Slepian, 1978). Different two-week data windows also yielded results consistent with our initial estimates.

4. Discussion

Where direct comparisons were available, (SCB1 and SCB3), the calibration results between procedures were consistent (Figure 4), although the drop procedure produced uncertainties typically half as large as those found with data post-processing methods. The results for the time constant at SCB2 also suggested consistency between techniques. Several potential sources of bias may have affected our results. The density of seawater was estimated here as 1028 kg/m^3, but varies throughout the oceanic with position and depth and could be 1035 kg/m^3 or higher at the seafloor in some locations (Talley et al., 2011), leading to different assumed pressure offsets. Uncertainties in the instrument depth, typically measured during deployment but not solved for through the re-location process, could yield large differences in the inferred sensitivity using Rayleigh wave transfer functions. A 5% increase in assumed water depth would lead to a roughly 5% decrease in the sensitivity factor. Variations in the velocity of sound in seawater or in local phase velocities could also alter the inferred sensitivity corrections, but moderate velocity perturbations (up to 2% in sound velocity or up to 10% in phase velocities) would impact the estimates by <1%. Calibrations obtained via the DPG drop, which are insensitive to local phase velocities, the average speed of sound in the water column, and absolute water depth, avoid some of these potential sources of bias.

The sensitivity of a DPG as documented here is a function of the response of the electronics, the mechanical response of the sensor, and a gain amplification term (see Supporting Information for details). The gain amplification term is defined in the software during deployment and should not contribute to the observed variations in sensitivity. Although the full range of the DPG is defined by the 24-bit analog-to-digital converter (i.e., -8388608 to 8388607 counts), the sensitivity of the electronics remains linear so long as the input signal is less than ± 3.0 V, corresponding to $\pm$ 7.32 million counts. The DPG signals remained below this threshold for the duration of the drop recordings. The mechanical response of the sensor, however, has proven difficult to constrain, as it includes a mechanical attenuation factor that is a function of the compressibility of the oil and the compliance of the chamber, both of which vary with pressure and temperature. The mechanical attenuation factor was initially estimated by Cox et al. (1984) to be 0.86, while Willoughby et al. (1993) measured a value of 0.924. Presently a value of 0.9 is assumed until this value can be better defined. Our results for the sensitivity corrections suggest that this value may be even less constrained than currently assumed, and may show considerable variation between instruments.

A number of factors may contribute to variations in the time constant between individual instruments. Within a DPG, the reference pressure is slowly relaxed to the ocean pressure by fluid flow through a

capillary leak in order to prevent large changes of pressure difference between the ocean and reference chamber. The time constant of the system is defined as

where η is the viscosity of the silicone oil, V_c is the volume of the reference chamber, L is the length of the cylinder, $(k_f + k_2)$ is the compressibility of the oil, Q is a constant, and r is the radius of the tube used for capillary flow. Cox et al. (1984) presented a value of 43 sec/rad but stated that the time constant is likely unknown to a factor of two. Much of the uncertainty stems from unpredictable behavior in the viscosity and compressibility of the reference oil at seafloor conditions. However, additional uncertainties may result from small imperfections in individual components, particularly the radius of the inner tube, which is raised to the fourth power. The introduction of silt or other small particulates into the oil during the initial construction of the devices may further alter the properties of the oil. In addition to the capillary leak, two pressure relief valves were introduced to the initial design to relieve pressure during periods in which the pressure signal exceeded the rating of the pressure transducer, for example during deployment and recovery of the instrument. These valves are sealed with o-ring and metal-to-metal closures. Although assumed to be impermeable, small leaks in these valves may decrease the relaxation time of the system and lower the time constant.

For this study, construction and installation of an individual DPG calibration mechanism was accomplished for less than $1,000, inclusive of material and time. These devices provide the only existing method to directly measure the in-situ response of an individual DPG at seafloor temperature and pressure conditions without the need to record specific signals (such as earthquakes and tidal peaks) on other sensors. While producing consistent results with alternative techniques, the drop data yield lower uncertainties and are not subject to a variety of assumptions that may influence post-processing results, including local phase velocities, station depth, and accurate tidal models as well as the seismometer instrument response. Equipping OBSs with these devices may prove a cost-efficient way to improve calibrations during future experiments. Planned repeat measurements with the same instruments during coming deployments will allow us to characterize whether DPG responses vary over time and between OBS deployments.

5. Conclusions

We presented the results from *in situ* tests designed to measure the sensitivity and long-period response of individual DPGs at seafloor temperatures and pressures by inducing a known pressure offset during the deployment. Our results demonstrate that both the sensitivity and time constant of nominally identical instruments can vary by a factor of two or greater, and suggest that DPGs should be calibrated individually. Our drop mechanisms are relatively inexpensive and can be added to existing OBS frameworks. Accurate calibrations of DPG data will permit improved observations of oceanographic and geophysical phenomena and will extend the utility of these data to lower frequency than previously possible.

Acknowledgments
Figures in this paper were generated using Generic Mapping Tools (Wessel et al., 2013) or with SolidWorks. We thank Jacques Lemire, Jon Berger, John Collins, Wayne Crawford and Spahr Webb for helpful discussions, and we thank the captain and crew of the R/V R. G. Sproul for two successful cruises. LeRoy Dorman provided assistance at sea and guidance through the data analysis. We thank Bruce Applegate and Liz Brenner for shore-side logistical help. Editor Paolo Diviacco, along with Flavio Accaino and an anonymous reviewer, contributed helpful comments that improved the manuscript. OSU tidal models and codes can be accessed at http://volkov.oce.orst.edu/tides/. Earthquake information was accessed from the USGS earthquake catalog (earthquake.usgs.gov/earthquakes/) via ObsPy (Beyreuther et al., 2010). Bathymetry data are available from https://topex.ucsd.edu/WWW_html/mar_topo.html. This project was made possible in part through funding from the UC Ship Funds program, the Paul G. Silver Young Scholar Research Enhancement Award, and the Cecil H. and Ida M. Green Foundation for Earth Sciences at IGPP. Raw seismic and pressure data reside at SIO and are used for student projects. The signals containing the DPG drop can be requested from Adrian Doran or Gabi Laske. Instrument specifics and calibrations are available at https://igppweb.ucsd.edu/~adoran.

References

An, C., Cai, C., Zheng, Y., Meng, L., & Liu, P. (2017). Theoretical solution and applications of ocean bottom pressure induced by seismic seafloor motion. *Geophysical Research Letters*, *44*, 10,272–10,281. https://doi.org/10.1002/2017GL075,137

Ball, J., Sheehan, A., Stachnik, J., Lin, F., & Collins, J. (2014). A joint Monte Carlo analysis of seafloor compliance, Rayleigh wave dispersion and receiver functions at ocean bottom seismic stations offshore New Zealand. *Geochemistry, Geophysics, Geosystems*, *15*, 5051–5068. https://doi.org/10.1002/2014GC005412

Bell, S. W., Forsyth, D., & Ruan, Y. (2015). Removing noise from the vertical component records of ocean-bottom seismometers: Results from Year One of the Cascadia Initiative. *Bulletin of the Seismological Society of America*, *105*(1), 300–313. https://doi.org/10.1785/0120140054

Berelson, W. M. (1991). The flushing of two deep-sea basins, southern California borderland. *Limnology and Oceanography*, *36*(6), 1150–1166.

Beyreuther, M., Barsch, R., Krischer, L., Megies, T., Behr, Y., & Wassermann, J. (2010). ObsPy: A Python toolbox for seismology. *Seismological Research Letters*, *81*(3), 530–533. https://doi.org/10.1785/gssrl.81.3.530

Bürgmann, R., & Chadwell, D. (2014). Seafloor Geodesy. *Annual Reviews of Earth and Planetary Science*, *42*, 509–534. https://doi.org/10.1146/annurev-earth-060313-054953

Cox, C., Deaton, T., & Webb, S. (1984). A deep-sea differential pressure gauge. *Journal of Atmospheric and Oceanic Technology*, *1*, 237–246.

Crawford, W., & Webb, S. (2000). Identifying and removing tilt noise from low-frequency (less than 0.1 Hz) seafloor vertical seismic data. *Bulletin of the Seismological Society of America*, *90*(4), 952–963. https://doi.org/10.1785/0119990121

Crawford, W., & Webb, S. (2002). Variations in the distribution of magma in the lower crust and at the Moho beneath the East Pacifc Rise at 9 and 10 degrees N. *Earth and Planetary Science Letters*, *203*, 117–130.

Crawford, W., Webb, S., & Hildebrand, J. (1991). Seafloor compliance observed by long-period pressure and displacement measurements. *Journal of Geophysical Research*, *96*(B10), 151–160.

Doran, A. K., & Laske, G. (2016). Infragravity waves and horizontal seafloor compliance. *Journal of Geophysical Research: Solid Earth*, *121*, 260–278. https://doi.org/10.1002/2015JB012511

Doran, A. K., & Laske, G. (2017). Ocean-bottom seismometer instrument orientations via automated Rayleigh-wave arrival angle measurements. *Bulletin of the Seismological Society of America*, *107*(2), 691–708. https://doi.org/10.1785/012016,165

Doran, A. K., & Laske, G. (2019). Seismic structure of marine sediments and upper oceanic crust surrounding Hawaii. *Journal of Geophysical Research: Solid Earth*, *124*, 2038–2056. https://doi.org/10.1029/2018JB016548

Dziewonski, A., & Anderson, D. (1981). Preliminary reference earth model. *Physics of the Earth and Planetary Interiors*, *25*(4), 297–356. https://doi.org/10.1016/0031-9201(81)90046-7

Egbert, G., & Erofeeva, S. (2002). Efficient inverse modeling of barotropic ocean tides. *Journal of Atmospheric and Oceanic Technology*, *19*(2), 183–204. https://doi.org/10.1175/1520-0426(2002)019<0183:EIMOBO>2.0.CO;2

Filloux, J. (1983). Pressure fluctuations on the open ocean floor off the Gulf of California: Tides, earthquakes, tsunamis. *Journal of Physical Oceanography*, *13*(5), 783–796. https://doi.org/10.1175/1520-0485(1983)013<0783:PFOTOO>2.0.CO;2

Godin, O., Zabotin, N., Sheehan, A., Yang, Z., & Collins, J. (2013). Power spectra of infragravity waves in a deep ocean. *Geophysical Research Letters*, *40*, 2159–2165. https://doi.org/10.1002/grl.50418

Godin, O. A., Zabotin, N. A., Sheehan, A. F., & Collins, J. A. (2014). Interferometry of infragravity waves off New Zealand. *Journal of Geophysical Research: Oceans*, *119*, 1103–1122. https://doi.org/10.1002/2013JC009395

Gusman, A. R., Sheehan, A. F., Satake, K., Heidarzadeh, M., Mulia, I. E., & Maeda, T. (2016). Tsunami data assimilation of Cascadia seafloor pressure gauge records from the 2012 Haida Gwaii earthquake. *Geophysical Research Letters*, *43*, 4189–4196. https://doi.org/10.1002/2016GL068368

Laske, G. (2011). The Hawaiian PLUME deployment: Lessons learned and recommendations for a Galapagos deployment. In *The Galapagos as a Laboratory for the Earth Sciences: American Geophysical Union Chapman Conference* (pp. 30–31). Puerto Ayora, Ecuador: American Geophysical Union. July 25 - 30.

Laske, G., Phipps Morgan, J., & Orcutt, J. (1999). First results from the Hawaiian Swell Pilot Experiment. *Geophysical Research Letters*, *26*(22), 3397–3400.

Laske, G., J. Phipps Morgan, and J. Orcutt (2007), The Hawaiian SWELL pilot experiment Evidence for lithosphere rejuvination from ocean bottom surface wave data, Geological Society of America, Special Paper 430.

Laske, G., & Widmer-Schnidrig, R. (2015). Treatise on Geophysics, vol. 1, chap. In *Theory and Observations: Normal Mode and Surface Wave Observations* (pp. 117–167). Oxford: Elsiever.

Melgar, D., & Boch, Y. (2013). Near-field tsunami models with rapid earthquake source inversions from land- and ocean-based observations: The potential for forecast and warning. *Journal of Geophysical Research: Solid Earth*, *118*, 5939–5955. https://doi.org/10.1002/2013JB010506

Nooner, S. L., & Chadwick, W. W. (2016). Inflation-predictable behavior and co-eruption deformation at Axial Seamount. *Science*, *354*(6831), 1399–1403. https://doi.org/10.1126/science.aah4666

Sasagawa, G., Cook, M. J., & Zumberge, M. A. (2016). Drift-corrected seafloor pressure observations of vertical deformation at Axial Seamount 2013-2014. *Earth and Space Science*, *3*, 381–385. https://doi.org/10.1002/2016EA000190

Saunders, J. K., & Haase, J. S. (2018). Augmenting onshore GNSS displacements with offshore observations to improve slip characterization for Cascadia Subduction Zone earthquakes. *Geophysical Research Letters*, *45*, 6008–6017. https://doi.org/10.1029/2018GL078233

Sheehan, A., Gusman, A., Heidarzadeh, M., & Satake, K. (2015). Array observations of the 2012 Haida Gwaii tsunami using Cascadia Initiative absolute and differential seafloor pressure gauges. *Seismological Research Letters*, *87*(3).

Sheehan, A. F., Z. Yang, D. Nicolsky, G. Mungov, and B. Eakins (2011), Exploring tsunamis with nontraditional dataset: Array recordings from temporary ocean-bottom seismic experiment, in Eos Trans. Fall meeting supplement, AGU.

Slepian, D. (1978). Prolate spheroidal wave functions, Fourier analysis and uncertainty, V, The discrete case. *Bell System Technical Journal*, *57*, 1371–1429.

Smith, W. H. F., & Sandwell, D. T. (1997). Global seafloor topography from satellite altimetry and ship depth soundings. *Science*, *277*, 1956–1962.

Talley, L. D., Packard, G. L., Emery, W. J., & Swift, J. H. (2011). *Descriptive Physical Oceanography: An Introduction (Sixth Edition)* (Vol. 6, 560 pp.). Boston: Elsevier. https://doi.org/10.1016/c2009-0-24322-4

Wahr, J. (1995). *Global Earth Physics: A Handbook of Physical Constants, vol. 1, chap. Earth Tides* (pp. 40–46). Washington, DC: American Geophysical Union.

Webb, S., & Crawford, W. (2010). Shallow-water broadband OBS seismology. *Bulletin of the Seismological Society of America*, *100*(4), 1770–1778. https://doi.org/10.1785/0120090203

Weeraratne, D. S., Forsyth, D. W., Yang, Y., & Webb, S. C. (2007). Rayleigh wave tomography beneath intraplate volcanic ridges in the South Pacific. *Journal of Geophysical Research*, *112*, B06303. https://doi.org/10.1029/2006JB004403

Wessel, P., Smith, W. H. F., Scharroo, R., Luis, J. F., & Wobbe, F. (2013). Generic Mapping Tools: Improved version released. *Eos Transactions, AGU*, *94*.

Wilcock, W. S. D., Stafford, K. M., Andrew, R. K., & Odom, R. I. (2014). Sounds in the ocean at 1-100 Hz. *Annual Review of Marine Science*, *6*, 117–140.

Willoughby, D. F., Orcutt, J. A., & Horwitt, D. (1993). A microprocessor-based ocean-bottom seismometer. *Bulletin of the Seismological Society of America*, *83*(1), 190–217.

Zha, Y., & Webb, S. (2016). Crustal shear velocity structure in the Southern Lau Basin constrained by seafloor compliance. *Journal of Geophysical Research: Solid Earth*, *121*, 3220–3237. https://doi.org/10.1002/2015JB012688